EXCITATION, PROPAGATION, AND DAMPING
OF ELECTRON BERNSTEIN WAVES
IN TOKAMAKS

A. K. Ram and S. D. Schultz

September 2000

Plasma Science & Fusion Center
Massachusetts Institute of Technology
Cambridge, Massachusetts 02139 USA

To appear in *Physics of Plasmas.*

Excitation, Propagation, and Damping of Electron Bernstein Waves in Tokamaks

A. K. Ram* and S. D. Schultz[†]

Plasma Science and Fusion Center, Massachusetts Institute of Technology, Cambridge, MA 02139

The conventional ordinary O-mode and the extraordinary X-mode in the electron cyclotron range of frequencies are not suitable for core heating in high-β spherical tokamak plasmas, like the National Spherical Torus Experiment [M. Ono, S. Kaye, M. Peng *et al.*, in *Proceedings of the 17th International Atomic Energy Agency Fusion Energy Conference,* (International Atomic Energy Agency, Vienna, 1999), Vol. 3, p. 1135], as they are weakly damped at high harmonics of the electron cyclotron frequency. However, electron Bernstein waves (EBW) can be effective for heating and driving currents in spherical tokamak plasmas. Power can be coupled to EBWs via mode conversion of either the X-mode or the O-mode. The two mode conversions are optimized in different regions of the parameter space spanned by the parallel wavelength and wave frequency. The conditions for optimized mode conversion to EBWs are evaluated analytically and numerically using a cold plasma model and an approximate kinetic model. From geometric optics ray tracing it is found that the EBWs damp strongly near the Doppler-broadened resonance at harmonics of the electron cyclotron frequency.

PACS numbers: 52.50.Gj, 52.35.Hr, 52.55.Hc, 52.40.Db

I. INTRODUCTION

There are distinct advantages to using radio-frequency waves in the electron cyclotron range of frequencies (ECRF) for heating fusion plasmas and for driving plasma currents. These advantages include the ease in coupling EC power into the plasma and the ability to readily adjust the launch angles. The major drawback, as far as conventional fusion tokamaks are concerned, is the unavailability of cw sources at very high frequencies (above the electron plasma frequency). The usually accepted procedure is to launch an extraordinary X-mode or an ordinary O-mode from the outboard side of a tokamak at a frequency above the cutoff frequencies of either mode inside the plasma. The X-mode or the O-mode then damp on electrons near the location of the electron cyclotron frequency f_{ce}, or its harmonics, inside the plasma. The modes are effectively damped near the fundamental and second harmonic of f_{ce}. At higher harmonics the damping is very weak so that neither of the two modes is a viable option for heating the plasma. This is especially true for spherical tokamaks (ST), like the National Spherical Torus Experiment (NSTX)[1] and the Mega Amp Spherical Tokamak (MAST).[2] While the availability of high-frequency sources is not a major concern, since the magnetic field in STs is significantly smaller than that in conventional tokamaks, the ratio of the electron plasma frequency f_{pe} to f_{ce} is well above one over most of the plasma cross-section. For instance, in NSTX high-β scenarios $f_{pe}/f_{ce} \sim 6$ in the core of the plasma. Thus, to access the core, the wave frequencies have to be near six times the core f_{ce} for which the damping of the X-mode and the O-mode is extremely weak. For low frequencies such that the fundamental or second harmonic of f_{ce} are inside the plasma, the O-mode and the X-mode are cutoff in the low-density outboard edge

region of the plasma and do not penetrate into the plasma core. A possible mechanism for by-passing this problem is to use the mode conversion of the slow X-mode to the electron Bernstein wave (EBW) at the upper hybrid resonance (UHR). The EBWs have no density cutoffs and, as we will show in this paper, the EBWs damp on electrons at the Doppler-broadened electron cyclotron resonance or its harmonics.

There are two techniques for coupling power to EBWs. The first technique involves the launching of an O-mode, from the outboard side, at such an angle (relative to the magnetic field) that the O-mode cutoff is spatially located at the same point as the left-hand cutoff of the slow X-mode.[3] Then the O-mode power is directly coupled to the slow X-mode, which in turn mode converts to EBWs at the upper hybrid resonance. This technique, referred to as the O-X-B mode conversion process, has been previously studied[3−7] and used successfully on Wendelstein 7-AS.[8] In the following we will show that effective O-X-B mode conversion requires conditions in addition to the coincidence of the O-mode and X-mode cutoffs. However, as shown in this experiment, if the launch angle of the O-mode is not chosen properly then there is no electron heating. The second technique is to launch the fast X-mode from the outboard side. The fast X-mode tunnels through the UHR and couples to the slow X-mode which, in turn, mode converts to EBWs at the UHR. This is referred to as the X-B mode conversion process. This process involves the X-mode right-hand cutoff, located towards the low-density side of the UHR, the UHR, and the left-hand cutoff of the slow X-mode, located towards the high-density side of the UHR. This triplet of cutoff-resonance-cutoff is similar to that encountered in the mode conversion of the fast Alfvén waves to the ion-Bernstein waves at the ion-ion hybrid resonance in plasmas with at least two ion species of different charge-to-

mass ratios.[9,10] In this paper we make use of the theory and the results obtained in Ref. 10 to study the X-B mode conversion. We find that the X-B conversion is efficient over a broad range of frequencies and launch angles. The X-B conversion has been alluded to before[11] and it has been identified in experiments in a linear plasma device,[12] but there has been no prior discussion of the details of this process. Some results of our analysis and computations have already appeared in conference publications .[13−16] Here in addition to showing the conditions for complete O-X-B mode conversion, we give the general theory of the X-B mode conversion process and discuss its relevance within the context of NSTX.

In this paper, we present analyses and computations on the excitation of EBWs by mode conversion of either the fast X-mode or the O-mode launched from the outboard side of the plasma, and illustrate the propagation and damping characteristics of EBWs in ST plasmas.

II. DISPERSION CHARACTERISTICS OF ELECTRON CYCLOTRON WAVES

We consider a slab geometry model for propagation along the equatorial plane of a toroidal plasma. Assuming a cold inhomogeneous plasma in a magnetic field pointing in the z-direction, the electric field $\vec{E} \sim e^{-i\omega t}$ inside the plasma is given by

$$\nabla \times \left(\nabla \times \vec{E} \right) = \frac{\omega^2}{c^2} \overline{\overline{K}} \cdot \vec{E} \tag{1}$$

where ω is the angular frequency, c is the speed of light, $\overline{\overline{K}}$ is the plasma permittivity tensor:

$$\overline{\overline{K}} = \begin{pmatrix} K_\perp & -iK_X & 0 \\ -iK_X & K_\perp & 0 \\ 0 & 0 & K_\parallel \end{pmatrix} \tag{2}$$

with

$$K_\perp = 1 - \frac{\omega_{pe}^2}{\omega^2 - \omega_{ce}^2} \tag{3}$$

$$K_X = -\frac{\omega_{ce}}{\omega} \frac{\omega_{pe}^2}{\omega^2 - \omega_{ce}^2} \tag{4}$$

$$K_\parallel = 1 - \frac{\omega_{pe}^2}{\omega^2} \tag{5}$$

ω_{pe} and ω_{ce} are functions of space and are the angular electron plasma and electron cyclotron frequencies, respectively. For waves in the electron cyclotron range of frequencies we can ignore the ion contribution to the plasma permittivity tensor. If we assume that there are no variations in the y-direction, the local dispersion relation is obtained by assuming that the electric field varies as $e^{(ik_\perp x + ik_\parallel z)}$ where $k_\perp$ and $k_\parallel$ are the components of the wave vector perpendicular and parallel to the magnetic field, respectively. Then from (1) we get:

$$K_\perp n_\perp^4 + \left[\left(K_\perp + K_\parallel \right) \left(n_\parallel^2 - K_\perp \right) + K_X^2 \right] n_\perp^2$$
$$+ \left\{ \left(n_\parallel^2 - K_\perp \right)^2 - K_X^2 \right\} K_\parallel = 0 \tag{6}$$

where $n_\parallel = ck_\parallel/\omega$ and $n_\perp = ck_\perp/\omega$. There are three cutoffs ($n_\perp = 0$) that arise from (6) and are given by:

$$\omega = \omega_O \equiv \omega_{pe} \tag{7}$$

$$\omega = \omega_L \equiv \frac{1}{2} \left[\left(\omega_{ce}^2 + \frac{4\omega_{pe}^2}{1 - n_\parallel^2} \right)^{1/2} + \omega_{ce} \right] \tag{8}$$

$$\omega = \omega_R \equiv \frac{1}{2} \left[\left(\omega_{ce}^2 + \frac{4\omega_{pe}^2}{1 - n_\parallel^2} \right)^{1/2} - \omega_{ce} \right] \tag{9}$$

which are the O-mode, the left-hand X-mode, and the right-hand X-mode cutoffs, respectively. The UHR is given by ($n_\perp = \infty$, $K_\perp = 0$):

$$\omega = \omega_{UHR} \equiv \sqrt{\omega_{pe}^2 + \omega_{ce}^2} \tag{10}$$

If we assume that the plasma inhomogeneity is along the x-direction, then for a given frequency and $n_\parallel = 0$, i.e., propagation across the magnetic field, the roots of (6) are plotted in Fig. 1. The locations of the O-mode cutoff (x_O), right-hand X-mode cutoff (x_R), left-hand X-mode cutoff (x_L), and the UHR (x_U) are identified explicitly. FX and SX identify the fast and the slow branches of the X-mode. The SX mode couples to the EBW near the upper hybrid resonance. This can be identified from solutions of the hot plasma dispersion relation where kinetic effects are included in the dielectric tensor.
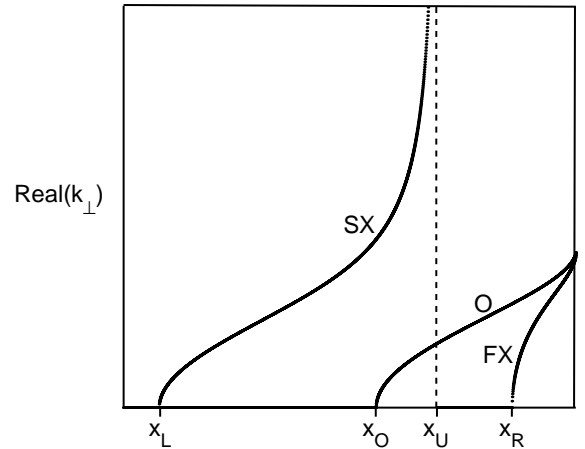

FIG. 1. The dispersion relation for ECRF modes. The cutoffs of the fast X-mode (FX), slow X-mode (SX), and the O-mode (O) are located at x_R (right-hand cutoff), x_L (left-hand cutoff), and x_O, respectively. x_U is the location of the upper hybrid resonance.

From Fig. 1 we note that the fast X-mode encounters a the right-hand cutoff (R) followed by the UHR. The

right-hand cutoff in close proximity to the UHR forms the classical Budden-type of mode conversion scenario.[17] This leads to a partial transmission of power to the slow X-mode and to partial absorption; the latter being equivalent to the fraction of incident power that is mode converted to the EBW. However, if the slow X-mode encounters the left-hand cutoff (L), the triplet of R–UHR–L forms a mode conversion resonator (i.e., a resonator containing mode conversion to EBW as an effective dissipation). This triplet of cutoff-resonance-cutoff is similar to that encountered in the mode conversion of fast Alfvén waves to ion-Bernstein waves at the ion-ion hybrid resonance .[9,10] In such a triplet resonator, one can, in principle, obtain complete mode conversion of the incident power to EBW. The local dispersion relation (6) is not valid for describing the propagation of waves through the cutoffs and resonances. For this we need to revert back to the differential equation (1).

III. THEORETICAL MODELLING OF X-B MODE CONVERSION

Assuming plasma inhomogeneity in the x-direction, uniformity in the y-direction, and the z-variation variation of the electric fields to be of the form $e^{(ik_\parallel z)}$, the wave equation (1) gives two coupled second-order ordinary differential equations in x for the field components E_y and E_z. If we consider the case of propagation transverse to the magnetic field ($k_\parallel = 0$) then the two equations decouple with one equation describing the propagation of the X-mode and the other describing the propagation of the O-mode. The X-mode propagation is given by:

$$\frac{d^2 E_y}{d\xi^2} + \Phi(\xi)E_y = 0 \tag{11}$$

where

$$\Phi(\xi) \equiv \frac{K_R K_L}{K_\perp} = \frac{K_\perp^2 - K_X^2}{K_\perp} \tag{12}$$

is the "scattering" potential, $\xi = (\omega/c)x$, and

$$K_R = K_\perp + K_X \tag{13}$$
$$K_L = K_\perp - K_X \tag{14}$$

Equation (12) has two cutoffs ξ_R and ξ_L corresponding to the location of the zeros of K_R and K_L, respectively, and a resonance at ξ_U where $K_\perp = 0$. By modelling the potential $\Phi(\xi)$ as is done in Ref. 10, a differential equation is obtained that is identical in form to that found, and solved, for the conversion of fast Alfvén waves to ion-Bernstein waves near the ion-ion hybrid resonance.[9,10] Carrying over our results from Ref. 10, we find the power mode conversion coefficient is

$$C = 4e^{-\pi\eta}(1 - e^{-\pi\eta})\cos^2\left(\frac{\phi}{2} + \theta\right) \tag{15}$$

where θ = phase of $\Gamma(-i\eta/2)$, ϕ is the phase difference between the slow X-mode propagating toward the L-cutoff and the reflected component propagating toward the UHR, and η is the Budden parameter. As in Ref. 10, η is obtained by expanding the potential Φ around the resonance, here the UHR, to find the location of ξ_R. This procedure leads to

$$\eta = \frac{\omega_{ce}L_n}{c}\frac{\alpha}{\sqrt{\alpha^2 + 2\frac{L_n}{L_B}}}\left[\frac{\sqrt{1+\alpha^2}-1}{\alpha^2 + \frac{L_n}{L_B}\sqrt{1+\alpha^2}}\right]^{1/2} \tag{16}$$

where

$$\alpha = \left[\frac{\omega_{pe}}{\omega_{ce}}\right]_{UHR} \tag{17}$$

the density scalelength L_n, and the magnetic field scalelength L_B are evaluated at the UHR. In the limit $L_B \gg L_n$

$$\eta \approx \frac{\omega_{ce}L_n}{c\alpha}\left[\sqrt{1+\alpha^2}-1\right]^{1/2} \tag{18}$$

For $\alpha \sim 1$:

$$\eta \approx \frac{1}{2}\left[\frac{\omega_{ce}L_n}{c}\right] \approx 293.5\,|BL_n|_{UHR} \tag{19}$$

where B is the local magnetic field in Tesla, and L_n is the scalelength in meters.

From (15) it is clear that the maximum possible power mode conversion, $C = 1$, is obtained if, simultaneously, $(\phi/2+\theta)$ is any integer multiple of π and $\exp(-\pi\eta) = 0.5$, i.e., $\eta \approx 0.22$. For this value of η we find, from (19) that

$$|BL_n|_{UHR} \approx 5.8 \times 10^{-4}\,\text{Tm} \tag{20}$$

This formula shows the advantage of the X-B mode conversion in spherical tokamaks which have lower magnetic fields compared to the conventional tokamaks; it also shows that a steep density gradient is required.

In order to illustrate our results we have chosen parameters that are NSTX-type for a high-β equilibrium.[18] The magnetic field, density, and temperature profiles along the equatorial plane (as a function of x) are given in Appendix A. For these NSTX-type parameters $C_{\max}$ as a function of the frequency $f = \omega/(2\pi)$ is plotted in Fig. 2. Here

$$C_{\max} = 4e^{-\pi\eta}\left(1 - e^{-\pi\eta}\right) \tag{21}$$

is the phase independent part of C from (15). Thus, $C_{\max}$ forms the envelope of the mode conversion coefficient C.

Note that complete mode conversion is possible for wave frequencies f around 16 GHz. In the range 13 GHz $\lesssim f \lesssim$ 18 GHz, $C_{\max} \geq 0.5$. This corresponds to η in the range $0.05 \lesssim \eta \lesssim 0.6$, or, equivalently, 1.3×10^{-4} T m $\lesssim |BL_n|_{UHR} \lesssim 1.6\times10^{-3}$ T m. For frequencies less than about 13 GHz the UHR is no longer inside the plasma and the X-B mode conversion is not possible.
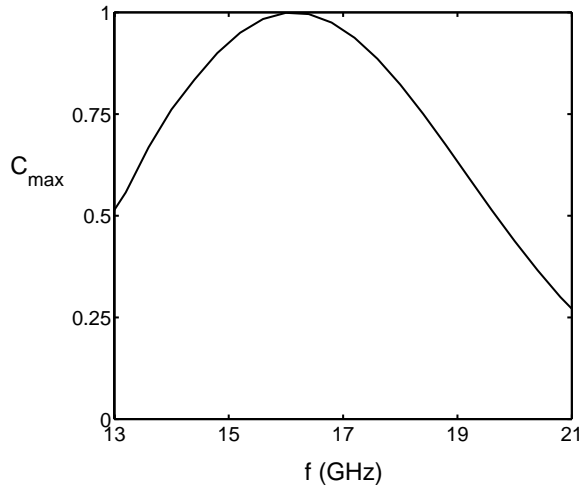
FIG. 2. Power mode conversion coefficient C_{max}, from Eq. (21), as a function of frequency for NSTX-type equilibrium profiles given in Appendix A.

IV. MODE CONVERSION (RESONANCE ABSORPTION) IN INHOMOGENEOUS, SHEARED MAGNETIC FIELD

The equilibria of high-β ST plasmas have poloidal magnetic fields that can be comparable to the toroidal magnetic fields in the outer part of the plasma. The shear in the magnetic field becomes important and has to be properly accounted for in the region where mode conversion takes place. We generalize our cold plasma, slab model to include both the poloidal magnetic field and shear. The inhomogeneity is assumed to be along x with arbitrary such variations for both the (toroidal) z-directed and the (poloidal) y-directed magnetic fields. The linearized field analysis is summarized in Appendix B. We find, from a local analysis, that the dispersion relation exhibits the same type of cutoff-resonance-cutoff triplet discussed earlier. Below, we give results from the numerical integration of the full complement of wave equations, Eqs. (B12) and (B13), describing the propagation of the O-mode and the X-mode in the mode conversion region.

Figure 3 shows the power mode conversion (resonance absorption) coefficient as a function of frequency, for NSTX-type equilibrium profiles, for $n_y = ck_y/\omega = 0$ and $n_z = ck_z/\omega = 0$ and 0.1. Superimposed is the curve obtained from Eq. (21) showing the theoretical maximum for the power mode converted to EBWs. The numerical results essentially follow the curve for C_{max} for frequencies below about 18 GHz. The difference between the theoretical maximum and the numerically evaluated results shows the effect of the phase factor in Eq. (15). Again, we note that mode conversion efficiencies $> 50\%$ are obtained for a broad range of frequencies. The power mode converted for $n_z = 0.1$ does not differ much from the result for $n_z = 0$. Furthermore, we find that a change in

the edge density of around 5% shifts the peak by about 1 GHz, but does not change its peak value or shape. Thus, mode conversion of the X-mode to EBWs in NSTX is both efficient and robust.

Figure 4 shows the X-B power mode conversion coefficient, for a source frequency of $f = 15$ GHz, as a function of n_z for $n_y = 0$. There is a broad range of low n_z's for which the mode conversion coefficient is greater than 50%.
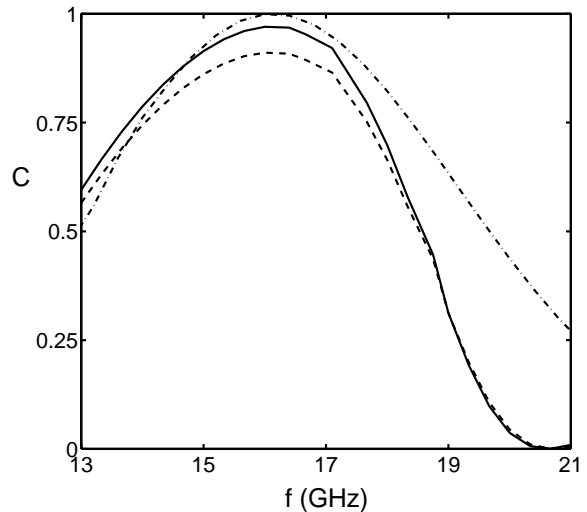

FIG. 3. Power mode conversion coefficient as a function of frequency for the resonance absorption model. The solid and dashed lines are for $n_z = 0$ and $n_z = 0.1$, respectively. The dot-dashed line is C_{max} of Fig. 2. The NSTX-type plasma and magnetic field equilibrium profiles are the same as for Fig. 2.

V. KINETIC DESCRIPTION OF MODE CONVERSION

The inclusion of kinetic effects due to finite temperature of the plasma resolves the singularity at the upper hybrid resonance. The resonance absorption is replaced by the kinetic EBW which propagates the energy away from the mode conversion region. A description of such a kinetic mode is much more complex and is not given by (B2) and (B3). Instead, one has to use the full complement of the Vlasov-Maxwell system of equations to determine the self-consistent evolution of the fields. For an inhomogeneous plasma this leads to an integral-differential equations whose solutions, even numerically, are difficult to obtain. Consequently, we seek an approximate description of the mode conversion process that includes the coupling of the kinetic EBW and the cold plasma modes. The derivation of such an approximate formulation, is given in Appendix C. Basically, we modify the
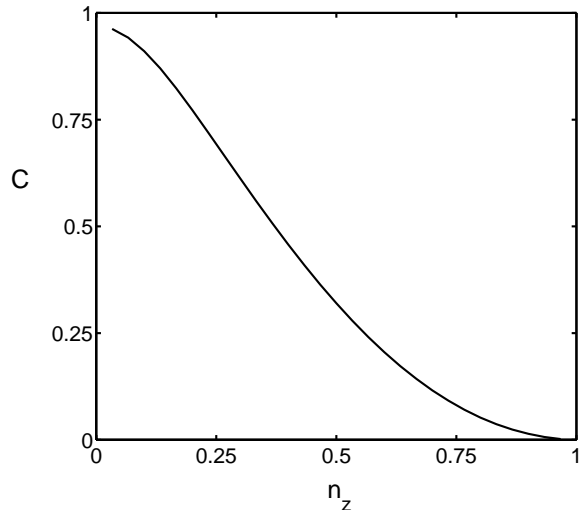
4

FIG. 4. Power mode conversion coefficient as a function of n_z for $f = 15$ GHz and $n_y = 0$. The NSTX-type plasma and magnetic field equilibrium profiles are the same as for Fig. 2.
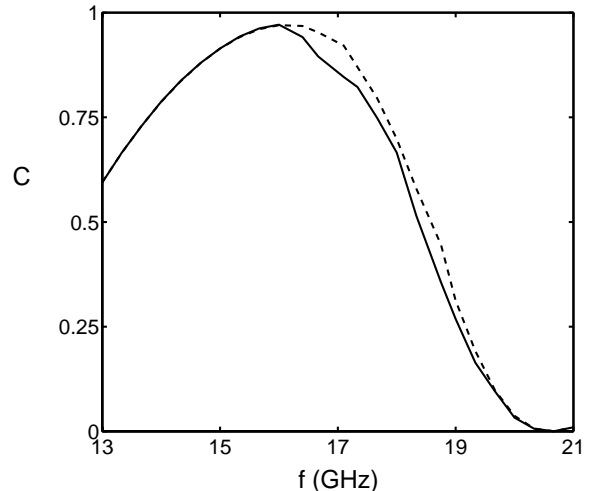

FIG. 5. Power mode conversion coefficient as a function of frequency. The solid line is the result from the kinetic description of the EBW while the dashed line is from the cold plasma resonance absorption model (solid line in Fig. 2). Both results are for $n_y = n_z = 0$. The NSTX-type plasma and magnetic field equilibrium profiles are the same as for Fig. 2.

cold plasma formulation to include the kinetic permittivity that is characteristic of the electrostatic EBW while retaining the general cold plasma description of Section IV and Appendix B. This process results in a set of six coupled first-order differential equations that include the coupling and propagation of the kinetic EBW and the cold plasma electromagnetic modes. The equation for the electromagnetic field components is given by Eqs. (C9) and (C10) Appendix B. These equations conserve the total (electromagnetic and kinetic) energy flow as given by (C11).

For NSTX-type parameters, Fig. 5 shows the power mode conversion coefficient, given by the ratio of the kinetic power flow in the EBW to the power input on the vacuum launched fast X-mode, as a function of frequency. This mode conversion coefficient is compared with the results from the cold plasma resonance absorption model. It is clear that the two results are in good agreement illustrating the validity of the cold plasma resonance absorption model as a representation of the power mode converted to EBWs. The results from the two models differ in the vicinity of the frequency (≈ 16.5 GHz) where the UHR passes from below $2f_{ce}$ to above – a transition that is immaterial in the cold-plasma resonance absorption model.

VI. MODE CONVERSION OF THE O-MODE TO THE EBW

There have been a number of theoretical studies on the mode conversion of a vacuum launched O-mode to the EBW.[3-7] The primary requirement for this mode conversion process to take place is that the O-mode cutoff be

near, or coincident with, the left-hand cutoff of the slow X-mode. This requires that the O-mode be launched at an oblique angle to the total magnetic field. The optimum $k_\parallel$ is that for which the two cutoffs are located at the same position. For oblique propagation, the left hand cutoff is given by Eq. (8) The optimum $n_{\parallel,opt}$ is when $\omega_L = \omega_{pe} \equiv \omega_O$, the O-mode cutoff in Eq. (7). This gives:

$$n_{\parallel,opt} = \frac{1}{\left(1 + \omega_{pe}/\omega_{ce}\right)^{1/2}} \qquad (22)$$

The modes obtained from the cold plasma dispersion relation for this optimum $n_{\parallel,opt}$ are illustrated in Fig. 6.

From this dispersion relation plot it is intuitively clear that power launched on the O-mode will directly couple to the slow X-mode at the left-hand cutoff. The slow X-mode then propagates towards the UHR where there is some resonance absorption, or, equivalently, mode conversion to EBW. However, from Fig. 6 it is clear that some of the power on the slow X-mode can tunnel through to the fast X-mode and propagate out to the edge of the plasma. The power transmission coefficient of the slow X-mode to the fast X-mode is given by:

$$T_X = e^{-\pi\eta} \qquad (23)$$

where η is as given in Eq. (16). Thus, in order to minimize the power transmitted we need $\eta > 1$. Consequently, for mode conversion of the O-mode to the EBW, we not only require an optimum angle of propagation,
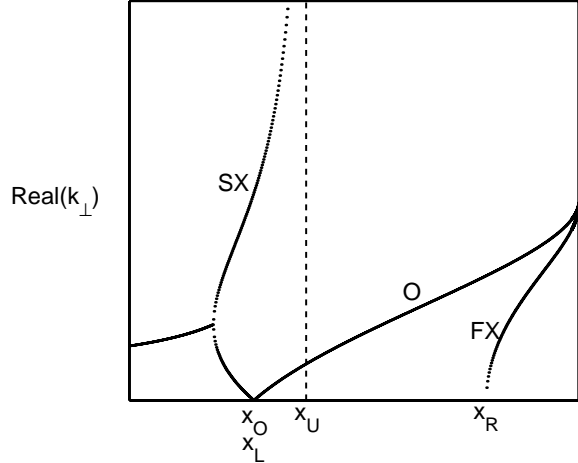
FIG. 6. The dispersion relation for ECRF modes for oblique propagation such that $x_L \approx x_O$

FIG. 7. Power mode conversion coefficient in as a function of n_z for $n_y = 0$. The solid, dashed, and dot-dashed lines are for source frequencies of 28, 14, and 21 GHz, respectively. The NSTX-type plasma and magnetic field equilibrium profiles are the same as for Fig. 2.

i.e., an optimum $k_\parallel$, but also $\eta > 1$. These two conditions are different from those for efficient mode conversion of the X-mode to EBW. This mode conversion process requires that $k_\parallel$ be small and that $\eta < 1$. For the same magnetic field, from Eq. (19) we find that the X-B mode conversion occurs closer to the edge of the plasma where the density scalelength is short, while the O-X-B mode conversion favors a longer density scalelength and, consequently, occurs deeper into the plasma.

The power mode conversion coefficient for the O-X-B process as a function of $n_\parallel$ is plotted for three different values of the wave frequency in Fig. 7. These results are obtained from the numerical solution of the cold plasma wave equations discussed in Appendix B.

For the frequency of 28 GHz, $n_{\parallel,opt} \approx 0.48$ and $C \approx 1$, while for 21 GHz, $n_{\parallel,opt} \approx 0.52$ and $C \approx 0.9$. The difference in the mode conversion coefficients is due to the power that is transmitted out on the X-mode. For the case of 28 GHz, $C \gtrsim 0.5$ for $0.4 \lesssim n_\parallel \lesssim 0.6$.

VII. DIRECT COUPLING TO EBW

For optimum X-B mode conversion it is evident from Eq. (20) that we need a short density scalelength that occurs, essentially, near the edge of the plasma. For NSTX-type parameters, the X-B mode conversion is optimized when the UHR resonance is within a few millimeters of the plasma-vacuum edge (see Fig. 12 in Appendix A). This distance is shorter than the free-space wavelength of the X-mode leading to the suggestion that effective direct coupling to EBW should be possible from an external slow wave structure that can be placed just inside of the confluence point of the EBW with the slow X-mode. The polarization of EBW, when near its confluence with the slow X-mode, is mainly $|E_x|$ so that external power ap-
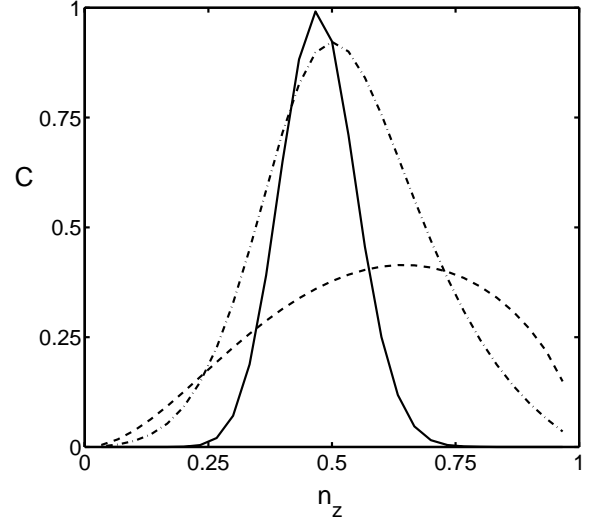
plied to a slow wave structure in close proximity to the plasma edge would excite the appropriate charge density perturbations that drive the EBW. The slow wave structure can also establish the desired $k_\parallel$-spectrum of the excited EBW which would lead to its heating and/or driving currents at desired locations to which it subsequently propagates in the plasma. In order to avoid any coupling to the slow X-mode it would be more effective to place the structure beyond the left-hand X-mode cutoff. For NSTX-type parameters this is near the UHR and is located inside the plasma near the plasma edge at a distance that is also short compared to the free-space wavelength. The coupling analysis, which is similar to the coupling analysis for lower hybrid and ion-Bernstein waves, will be presented elsewhere.

VIII. PROPAGATION AND DAMPING OF EBWS

The propagation characteristics of EBWs are studied using the code GORAY which follows ray trajectories in a hot Maxwellian plasma using the geometric optics approximation. This code has been previously used to study the propagation and damping of ion-Bernstein waves.[19] The ray trajectories of EBWs are determined starting at a location beyond the mode conversion region near the UHR where the geometric optics approximation is valid. Within the mode conversion region we have to use the differential equation formalism discussed above. Furthermore, while the spatially narrow mode conversion region can be treated within the slab geometry approx-

imation, the propagation studies of EBWs require a full representation of the toroidal plasma. Toroidal effects play a significant role in the propagation of EBWs. For NSTX-type parameters discussed in Appendix A, Fig. 8 shows the trajectories of two EBW rays over the minor cross-section of the plasma. The two rays are distinguished by the starting spatial location of the rays. The first ray is started on the equatorial plane while the second ray is started slightly above this plane. The rays are followed until they are completely damped. Figure 9 shows the normalized energy density as a function of x along the two rays. The energy density is normalized to be 1 at the starting location of the two rays. We find that the rays damp on electrons due to cyclotron damping at the Doppler-broadened second harmonic electron cyclotron resonance. There is no damping of EBWs prior to reaching this Doppler-broadened resonance.

FIG. 9. Normalized energy density along the two rays of Fig. 8. The energy density is normalized to be one at the initial starting location of the rays on the right-hand side.
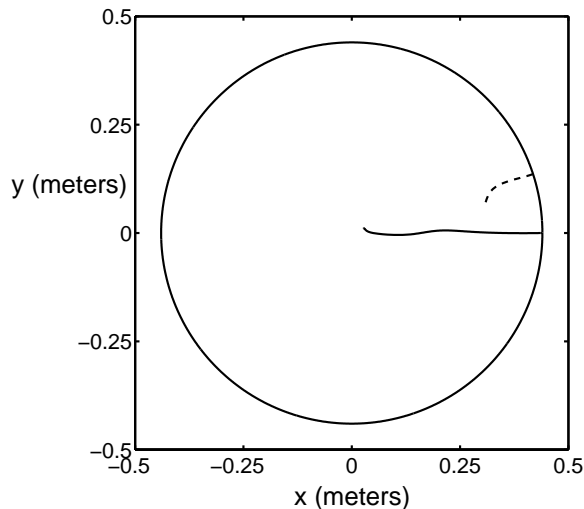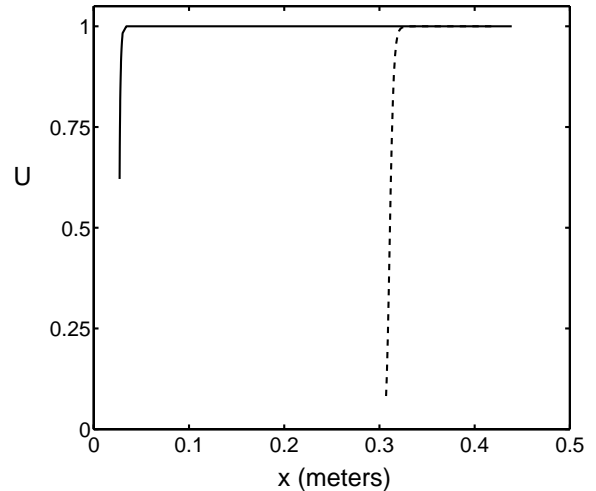

FIG. 8. Poloidal projection of two EBW ray trajectories for NSTX-type parameters. The outboard edge of the plasma is at $x = 0.44$ m and the center is at $x = 0$. The first ray (solid line) is started on the equatorial plane $\theta = 0$, where θ is the poloidal angle, while the second ray (dashed line) is started slightly above the equatorial plane at $\theta = 0.1\pi$.

The two rays damp at very different spatial locations because of the evolution of $n_\parallel$ along the rays. Figure 10 shows the $n_\parallel$ evolution of both rays which were initially started with $n_\parallel = 0.1$. For the ray started on the equatorial plane, the change in $n_\parallel$ is relatively small compared to the ray started above the equatorial plane. The large change in $n_\parallel$ coupled with a nearly flat magnetic field profile (see Appendix A) lead to the damping of the second ray well away from the actual spatial location of the second harmonic electron cyclotron resonance. This resonance is located near $x = 0$ in close proximity to the location where the first ray damps on electrons. From Ref. 19 we know that the change in $n_\parallel$ along the ray has the following dependencies:
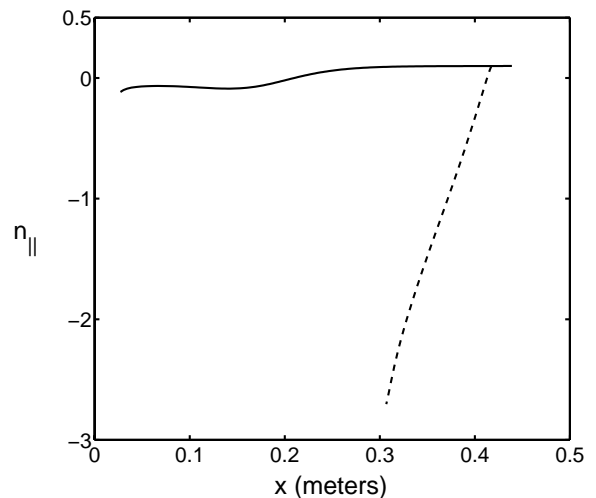

FIG. 10. The parallel wave numbers $n_\parallel$ along the two rays of Fig. 8. The two rays are started off initially with $n_\parallel = 0.1$ at the right-hand side near $x = 0.44$ m.

$$\Delta n_\parallel \; \propto \; \sin\left(\theta\right) \left| \frac{B_p}{B} \right| \mathrm{sign}\left(n_\perp\right) \qquad (24)$$

where θ is the poloidal angle measured from the center of the plasma with $\theta = 0$ being the outboard side of the equatorial plane, B_p is the poloidal magnetic field, B is the total magnetic field, and $n_\perp$ is the perpendicular wave number of the EBW. From (24) it is clear that the change in $n_\parallel$ should be small for rays near the equatorial plane ($\theta \approx 0$). Since towards the outer half of the plasma $|B_p| \approx |B|/2$ (see Appendix A), the change in $n_\parallel$ for rays away from the equatorial plane can be significant. Figure 10 shows that this is indeed the case for the ray which is launched off the equatorial plane. Since EBWs are backward waves $\mathrm{sign}(n_\perp) < 0$ and, subsequently, $\Delta n_\parallel < 0$ in the upper-half section of the plasma. $\Delta n_\parallel > 0$ in the lower-half section of the plasma.

From the results shown in Figs. 8 and 9 it is evident that EBWs damp locally and strongly near the Doppler-shifted harmonic of the electron cyclotron resonance frequency. Furthermore, we find that the waves damp on electrons. These properties make EBWs an attractive candidate for localized electron heating in spherical tokamaks.

IX. CONCLUSIONS

A detailed theoretical and computational analysis of mode conversion to electron Bernstein waves in NSTX-type spherical tokamaks show that the two mode conversion processes, X-B and O-X-B, are optimized in different regions of the parameter space spanned by the parallel (to the magnetic field) wavenumbers $n_\parallel$ and the wave frequency. The X-B mode conversion is optimized for low $n_\parallel$'s and frequencies such that the upper hybrid resonance is located closer the edge of the plasma where the density scalelengths are short. The O-X-B mode conversion is optimized for $n_\parallel \sim 0.5$ and for frequencies such that the upper hybrid resonance is located farther into the plasma where the density scalelenghts are long and the coupling to the fast X-mode is weak. Thus, the X-B mode conversion process operates more efficiently at frequencies lower than that for the O-X-B mode conversion.

In the low frequency regime of the X-B mode conversion, the upper hybrid resonance is located at a distance from the edge of the plasma that is short compared to the free-space wavelength of the X-mode. It may be possible to couple directly to EBWs at the edge using a slow wave structure. Further studies on this coupling process are in progress.

A geometrical optics ray trajectory analysis shows that the EBWs damp effectively on electrons in spatially localized regions near the Doppler-shifted harmonic of the electron cyclotron frequency. However, the spatial location of the damping can change depending on the poloidal launch angle of the EBWs. For rays near the equatorial plane the damping is closer to the spatial location of the

harmonic of the electron cyclotron frequency. For rays that are launched away from the equatorial plane the large changes in $n_\parallel$ can lead to significant deviations in the location of the damping region. Since the change in $n_\parallel$ is determined by whether the EBWs are launched above or below the equatorial plane, the velocity-space interaction of the EBWs with the electron distribution function can be controlled by an appropriate choice of the launch position.

APPENDIX A: CUTOFF AND RESONANCE FREQUENCIES FOR NSTX-TYPE PARAMETERS

The NSTX-type high-β equilibrium that we have used in our calculations is as follows.[18] The Shafranov-shifted major radius is $R = 1.05$ m, the minor radius is $a = 0.44$ m, the peak electron density is $n_0 = 3 \times 10^{19}$ m^{-3}, the peak electron temperature is $T_0 = 3$ keV, the density profile is $n_e = n_E + (n_0 - n_E)(1 - x^2/a^2)^{1/2}$, and the temperature profile is $T_e = T_E + (T_0 - T_E)(1 - x^2/a^2)^2$, where n_E and T_E are the edge density and temperature, respectively, with $n_E/n_0 = 0.02$ and $T_0/T_E = 0.02$. The magnetic field profile is taken to be that shown below in Fig. 11

In Fig. 12 we plot the frequencies of the various cutoffs and resonances along equatorial plane of the NSTX-type plasma mentioned in the text.

For the equilibrium used in the ray tracing calculations we have assumed that the density and temperature profiles are $(1 - r^2/a^2)^{1/2}$ and $(1 - r^2/a^2)^2$, respectively, where r is the radial coordinate. The poloidal and toroidal magnetic fields are, respectively, modelled as:

$$B_\theta = \frac{B_{\theta 0}(r)}{1 + (r/R)\cos\theta} \qquad (A1)$$

$$B_\phi = \frac{B_{\phi 0}}{1 + (r/R)\cos\theta} \qquad (A2)$$

where θ is the poloidal angle, $B_\phi 0 = 0.26$ Tesla, and $B_{\theta 0}(r)$ has the profile of B_y in Fig. 11.

FIG. 11. The magnitudes of the poloidal component B_y (dot-dashed), the toroidal component B_z (dashed), and the total magnetic field B (solid line) in Tesla as a function of the minor radius. $x = 0$ is the center of the plasma and $x = 0.44$ m is the outside edge of the plasma.
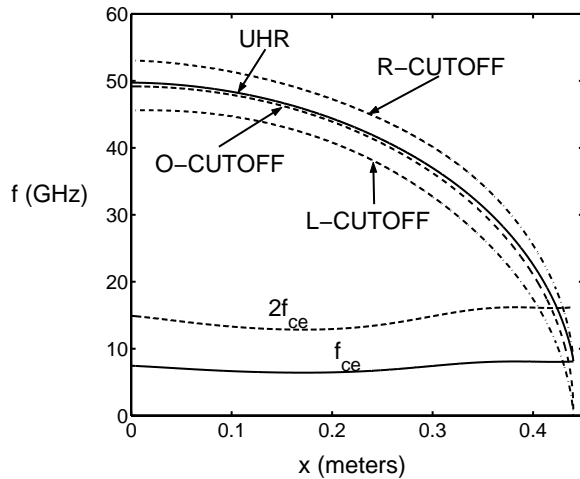
FIG. 12. The frequencies corresponding to the UHR, the right-hand cutoff, the left-hand cutoff, the O-mode cutoff, and the fundamental and second harmonic of f_{ce} as a function of distance along the plasma cross-section

APPENDIX B: FIELD EQUATIONS IN A COLD, INHOMOGENEOUS PLASMA

We consider a stationary, neutral, electron-ion plasma equilibrium in an inhomogeneous, sheared magnetic field:

$$\vec{B}_0(x) = \hat{y}B_0(x)\sin\Psi(x) + \hat{z}B_0(x)\cos\Psi(x) \qquad (B1)$$

where Ψ is the angle between $\vec{B}_0$ and the z-axis in a cartesian (x, y, z) coordinate system, and x, y, and z are the radial, poloidal, and toroidal components, respectively. The equilibrium plasma density is assumed to vary with x: $n_0 = n_0(x)$. For the high frequencies in the range of electron cyclotron frequencies we can neglect the dynamics of the ions. Ignoring collisions, the linearized cold-plasma dynamics of the electrons is described by the continuity equation

$$\frac{\partial n_1}{\partial t} + \nabla \cdot (n_0 \vec{v}_1) = 0 \qquad (B2)$$

and the non-relativistic momentum equation

$$m_e \frac{\partial \vec{v}_1}{\partial t} = -e(\vec{E}_1 + \vec{v}_1 \times \vec{B}_0) \qquad (B3)$$

where m_e is the electron mass, and n_1, v_1, and E_1 are the first-order perturbations in the electron density, the electron fluid velocity, and the electric field, respectively. Assuming a time dependence of the form $e^{-i\omega t}$ for all the perturbation parameters, the perturbed current density $\vec{J}_1 = -en_0\vec{v}_1$ is given as a function of $\vec{E}_1$ by solving (B3) for $\vec{v}_1$. The result can be expressed in terms of the susceptibility tensor $\overset{\leftrightarrow}{\chi}(x, \omega)$ defined by

$$\vec{J}_1 = -i\omega\epsilon_0 \overset{\leftrightarrow}{\chi} \cdot E_1 \qquad (B4)$$

where ϵ_0 is the dielectric constant of free space. We find that

$$\overset{\leftrightarrow}{\chi} = \frac{-\alpha^2}{(1-\beta^2)} \begin{pmatrix} 1 & -i\beta_c & i\beta_s \\ i\beta_c & 1-\beta_s^2 & -\beta_s\beta_c \\ -i\beta_s & -\beta_s\beta_c & 1-\beta_c^2 \end{pmatrix} \qquad (B5)$$

where $\alpha^2 = \omega_{pe}^2(x)/\omega^2$, $\beta = \omega_{ce}(x)/\omega$, $\beta_c = \beta\cos\Psi(x)$, and $\beta_s = \beta\sin\Psi(x)$. Substituting for the current density into Maxwell's equation for the first-order fields, we get

$$\nabla \times \vec{E}_1 = i\omega\vec{B}_1 \qquad (B6)$$

$$\nabla \times \vec{B}_1 = -i\frac{\omega}{c^2} \overset{\leftrightarrow}{K} \cdot \vec{E}_1 \qquad (B7)$$

where the permittivity tensor $\overset{\leftrightarrow}{K}(x, \omega)$ is

$$\overset{\leftrightarrow}{K} = \overset{\leftrightarrow}{I} + \overset{\leftrightarrow}{\chi} = \begin{pmatrix} K_{xx} & \chi_{xy} & \chi_{xz} \\ -\chi_{xy} & K_{yy} & \chi_{yz} \\ -\chi_{xz} & \chi_{yz} & K_{zz} \end{pmatrix} \qquad (B8)$$

9

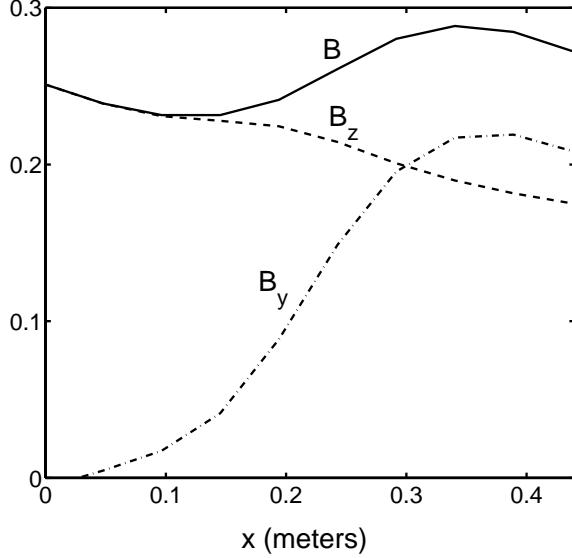and $\overset{\leftrightarrow}{I}$ is the second-rank identity tensor. Equations (B6) and (B7) can be used to derive a set of first-order differential equations for the self-consistent electromagnetic fields. We choose the field (column) vector $\vec{F}_c$ such that its transpose (row) vector is

$$\vec{F}_c^T = [E_y \ E_z \ (-cB_y) \ cB_z] \qquad (B9)$$

Then the time-averaged electromagnetic energy flow density is given by

$$\langle \vec{s}_{em} \rangle = \frac{1}{4} \sqrt{\frac{\epsilon_0}{\mu_0}} \ \vec{F}_c^\dagger \cdot \overset{\leftrightarrow}{M} \cdot \vec{F}_c \ \hat{x} \qquad (B10)$$

where the dagger superscript denotes the complex-conjugate transpose and

$$\overset{\leftrightarrow}{M} = \begin{pmatrix} 0 & 0 & 0 & 1 \\ 0 & 0 & 1 & 0 \\ 0 & 1 & 0 & 0 \\ 1 & 0 & 0 & 0 \end{pmatrix} \ . \qquad (B11)$$

We assume that the plasma equilibrium is uniform in y and z so that the fields vary as $e^{ik_y y + ik_z z}$. Then Eqs. (B6) and (B7) can be written as

$$\frac{d\vec{F}_c}{d\xi} = i \overset{\leftrightarrow}{A}_c \cdot \vec{F}_c \qquad (B12)$$

where $\xi = \omega x / c$,

$$\overset{\leftrightarrow}{A}_c = \frac{1}{K_{xx}} \begin{bmatrix} -n_y \chi_{xy} & -n_y \chi_{xz} & -n_y n_z & K_{xx} - n_y^2 \\ -n_z \chi_{xy} & -n_z \chi_{xz} & K_{xx} - n_z^2 & -n_y n_z \\ a_1 & a_2 & n_z \chi_{xz} & n_y \chi_{xz} \\ a_3 & a_1 & n_z \chi_{xy} & n_y \chi_{xy} \end{bmatrix} \qquad (B13)$$

$a_1 = K_{xx}(\chi_{yz} + n_y n_z) + \chi_{xy}\chi_{xz}$, $a_3 = K_{xx}(K_{zz} - n_y^2) + \chi_{xz}^2$, $a_3 = K_{xx}(K_{yy} - n_z^2) + \chi_{xy}^2$, $n_y = (ck_y/\omega)$, and $n_z = (ck_z/\omega)$. It can be easily seen that $\overset{\leftrightarrow}{M} \cdot \overset{\leftrightarrow}{A}$ is Hermitian so that the time-averaged energy flow density in x is conserved, i.e.,

$$\frac{d}{d\xi}(\vec{F}_c^\dagger \cdot \overset{\leftrightarrow}{M} \cdot \vec{F}_c) = 0 \ . \qquad (B14)$$

APPENDIX C: KINETIC FIELD EQUATIONS

Here we formulate the mode conversion equations that include the kinetic electron Bernstein wave and the cold-plasma modes in the inhomogeneous equilibrium described in Appendix B.

In a homogeneous plasma, the electrostatic EBW is associated with the K_{xx} component of the kinetic (Vlasov) permittivity tensor. For a weakly damped electrostatic wave, the dominant component of the kinetic energy flow density is given by Ref. 20

$$\langle \vec{s}_K \rangle = -\frac{1}{4} \ \epsilon_0 \omega \ \frac{\partial K_{\alpha\beta}^K}{\partial \vec{k}} \ E_\alpha E_\beta^* \qquad (C1)$$

where $\overset{\leftrightarrow}{K}{}^K$ is the Hermitian part of the kinetic permittivity tensor. Since we are interested in a full wave characterization of the EBW between the fundamental and second electron cyclotron harmonics, where the Doppler-shifted cyclotron damping is negligible, it is sufficient to expand the kinetic susceptibility χ_{xx}^K to second order in $(k_\perp v_{Te}/\omega_{ce})$ where $v_{Te} = \sqrt{(\kappa T_e/m_e)}$ is the electron thermal velocity. For a Maxwellian electron distribution function:[21]

$$\chi_{xx}^K \approx \chi_{xx} + \tilde{\chi} n_x^2 \qquad (C2)$$

where χ_{xx} is the cold-plasma susceptibility (see Appendix B), $n_x = (ck_x/\omega)$, and

$$\tilde{\chi} = \frac{-3\omega_{pe}^2 \omega^2}{(\omega^2 - \omega_{ce}^2)(\omega^2 - 4\omega_{ce}^2)} \left(\frac{v_{Te}}{c} \right)^2 \ . \qquad (C3)$$

For χ_{xx}^K as a slowly varying function of x, the conservation of the kinetic energy flow density in x,

$$\frac{d}{d\xi} \left(\frac{\partial K_{xx}^K}{\partial n_x} |E_x|^2 \right) = 0 \qquad (C4)$$

requires that the inhomogeneous representation of the kinetic EBW mode be related to its homogeneous, local representation $K_{xx}^K E_x$ as follows:[22]

$$K_{xx}^K E_x \rightarrow K_{xx} E_x - \frac{d}{d\xi} \left(\tilde{\chi} \frac{dE_x}{d\xi} \right) \qquad (C5)$$

So the prescription for formulating the coupling between the cold plasma electromagnetic modes and the kinetic EBW is to:

(a) introduce the modification to $K_{xx}E_x$ in Maxwell's equation (B7) according to (C5); and

(b) choose a field vector $\vec{F}_K$ for the new, self-consistent, electromagnetic fields described by Eqs. (B6) and (B7), with the appropriately modified $\overset{\leftrightarrow}{K}$, to obtain a set of first-order differential equations in x.

The field vector $\vec{F}_K$ is chosen such that its transpose (row) is

$$\vec{F}_K^T = [E_x \ E_y \ E_z \ (i\tilde{\chi} E_x') \ cB_z \ (-cB_y)] \qquad (C6)$$

where $E_x' = (dE_x/d\xi)$ The *total (electromagnetic and kinetic)* time-averaged energy flow density is given by:

$$\langle \vec{s} \rangle = \frac{1}{4} \sqrt{\frac{\epsilon_0}{\mu_0}} \ \vec{F}_K^\dagger \cdot \overset{\leftrightarrow}{R} \cdot \vec{F}_K \ \hat{x} \qquad (C7)$$

where

$$
\overset{\leftrightarrow}{R} =
\begin{bmatrix}
 & & & | & 1 & 0 & 0 \\
 & 0 & & | & 0 & 1 & 0 \\
 & & & | & 0 & 0 & 1 \\
- & - & - & - & - & - & - \\
1 & 0 & 0 & | & & & \\
0 & 1 & 0 & | & & 0 & \\
0 & 0 & 1 & | & & &
\end{bmatrix} .
\tag{C8}
$$

Following the procedure in Appendix B, the evolution of the fields is given by:

$$
\frac{d\vec{F}_K}{d\xi} = i \overset{\leftrightarrow}{A}_K \cdot \vec{F}_K
\tag{C9}
$$

where

$$
\overset{\leftrightarrow}{A}_K =
\begin{bmatrix}
0 & 0 & 0 & -\tilde{\chi}^{-1} & 0 & 0 \\
n_y & 0 & 0 & 0 & 1 & 0 \\
n_z & 0 & 0 & 0 & 0 & 1 \\
K_{xx} & \chi_{xy} & \chi_{xz} & 0 & n_y & n_z \\
-\chi_{xy} & K_{yy} - n_z^2 & \chi_{yz} + n_y n_z & 0 & 0 & 0 \\
-\chi_{xz} & \chi_{yz} + n_y n_z & K_{zz} - n_y^2 & 0 & 0 & 0
\end{bmatrix}
\tag{C10}
$$

It can be readily verified that $\overset{\leftrightarrow}{R} \cdot \overset{\leftrightarrow}{A}_K$ is Hermitian so that the total time-averaged energy flow density in x is conserved, i.e.,

$$
\frac{d}{d\xi}(\vec{F}_K^\dagger \cdot \overset{\leftrightarrow}{R} \cdot \vec{F}_K) = 0 .
\tag{C11}
$$

For $\tilde{\chi} = 0$ (the cold plasma limit), Eq. (C10) has a singular term in its first row. However, the cold plasma limit is readily obtained from Eqs. (C9, C10). Using Eq. (C6) it is clear that the first equation in (C9, C10) is trivial and independent of $\tilde{\chi}$. The fourth equation with $\tilde{\chi} = 0$ allows us to solve for E_x in terms of E_y, E_z, cB_z, and cB_y. Substituting this for E_x in the remaining four equations gives exactly the results in Eqs. (B12, B13). There is also an alternative formulation in which, if we restrict ourselves to just the (transposed) electric field vector $\vec{E}_1^T = (E_x\ E_y\ E_z)$, the elimination of $\vec{B}_1$ between (B6) and (B7) results in:

$$
\overset{\leftrightarrow}{D}_{op} \cdot \vec{E}_1 = 0
\tag{C12}
$$

where

$$
\overset{\leftrightarrow}{D}_{op} =
$$

$$
\begin{bmatrix}
\begin{aligned} n_y^2 + n_z^2 - K_{xx} \\ + \frac{d}{d\xi}\tilde{\chi}\frac{d}{d\xi} \end{aligned} & in_y\frac{d}{d\xi} - \chi_{xy} & in_z\frac{d}{d\xi} + \chi_{xz} \\
in_y\frac{d}{d\xi} + \chi_{xy} & -\frac{d^2}{d\xi^2} + n_z^2 - K_{yy} & -n_y n_z - \chi_{yz} \\
in_z\frac{d}{d\xi} - \chi_{xz} & -n_y n_z - \chi_{yz} & -\frac{d^2}{d\xi^2} + n_y^2 - K_{zz}
\end{bmatrix}
\tag{C13}
$$

In the limit $\tilde{\chi} \to 0$, (C12) with (C13) are non-singular and equivalent to the cold plasma formulation in (B12) with (B13). The clear disadvantage of this formulation is that the coupled ordinary differential equations include derivatives of the susceptibility tensor elements. This makes the numerical procedures more cumbersome.

Finally, we remark that the above approximate representation of EBWs for ω_{UHR} in the vicinity of $2\omega_{ce}$ can be extended to include the case when ω_{UHR} is in the vicinity of $3\omega_{ce}$. This entails expanding the kinetic susceptibility to fourth order in $k_\perp v_{Te}/\omega_{ce}$, giving

$$
\chi_{xx}^K \approx \chi_{xx} + \tilde{\chi}n_x^2 + \tilde{\tilde{\chi}}n_x^4
\tag{C14}
$$

where

$$
\tilde{\tilde{\chi}} = -\frac{15\omega_{pe}^2\omega^4}{(\omega^2 - \omega_{ce}^2)(\omega^2 - 4\omega_{ce}^2)(\omega^2 - 9\omega_{ce}^2)} \left(\frac{v_{Te}}{c}\right)^4
\tag{C15}
$$

This leads to an eighth order differential equation for the fields.

[*] Electronic mail: abhay@psfc.mit.edu

[†] Present address: Raytheon Corporation, Marlboro, MA.

[1] M. Ono, S. Kaye, M. Peng *et al.*, in *Proceedings of the 17th International Atomic Energy Agency Fusion Energy Conference,* (International Atomic Energy Agency, Vienna, 1999), Vol. 3, p. 1135.

[2] A. Sykes, in *Proceedings of the 17th International Atomic Energy Agency Fusion Energy Conference,* (International Atomic Energy Agency, Vienna, 1999), Vol. 1, p. 129.

[3] J. Preinhaelter and V. Kopecky, J. Plas. Phys. **10**, 1 (1973).

[4] H. Weitzner and D. B. Batchelor, Phys. Fluids **22**, 1355 (1979).

[5] S. Nakajima and H. Abe, Phys. Lett. A **124**, 295 (1987).

[6] F. R. Hansen, J. P. Lynov, C. Mardi, and V. Petrillo, J. Plas. Phys. **39**, 319 (1988).

[7] E. Mjolhus, J. Plasma Phys. **31**, 7 (1984).

[8] H. P. Laqua, V. Erkmann, H. J. Hartfuss, and H. Laqua, Phys. Rev. Lett. **78**, 3467 (1997).

[9] V. Fuchs, A. K. Ram, S. D. Schultz, A. Bers, and C. N. Lashmore-Davies, Phys. Plas. **2**, 1637 (1995).

[10] A. K. Ram, A. Bers, S. D. Schultz, and V. Fuchs, Phys. Plas. **3**, 1976 (1996).

[11] S. Nakajima and H. Abe, Phys. Rev. A **38**, 4373 (1988).

[12] H. Sugai, Phys. Rev. Lett. **47**, 1899 (1981).

[13] A. K. Ram, in *Proceedings of the 13th Topical Conference on Radio Frequency Power in Plasmas (A.I.P. Conference Proceedings No. 485)*, edited by S. Bernabei and F. Paoletti (American Institute of Physics, New York, 1999), pp. 375–382.

[14] S. D. Schultz, A. K. Ram, and A. Bers, in *Proceedings of the 17th International Atomic Energy Agency Fusion Energy Conference,* (International Atomic Energy Agency, Vienna, 1999), Vol. 2, p. 667.

[15] A. Bers, A. K. Ram, and S. D. Schultz, in *Proceedings of the Second Europhysics Topical Conference on RF Heating and Current Drive of Fusion Devices,* edited by J. Jacquinot, G. Van Oost, and R. R. Weynants (European Physical Society, Petit-Lancy, 1998), Vol. 22A, pp. 237–240.

[16] K. C. Wu, A. K. Ram, A. Bers, and S. D. Schultz, in *Proceedings of the 12th Topical Conference on RF Power in Plasmas, AIP Conference Proceedings 403* edited by P. M. Ryan and T. Intrator (American Institute of Physics, New York, 1997) pp. 207–210.

[17] K. Budden, *The Propagation of Radio Waves,* (Cambridge University Press, Cambridge, 1985), pp. 596–602.

[18] Plasma equilibrium and B-field profiles provided by Dr. R. Majeski of the Princeton Plasma Physics Laboratory, Princeton, New Jersey.

[19] A. K. Ram and A. Bers, *Phys. Fluids B* **3**, 1059 (1991).

[20] See, for example, W. P. Allis, S. J. Buchsbaum, and A. Bers, *Waves in Anisotropic Plasmas*, (Massachusetts Institute of Technology Press, Cambridge, 1963), Sec. 8.5; A. Bers, in *Plasma Physics — Les Houches 1972*, edited by C. DeWitt and J. Peyraud (Gordon and Breach, New York, 1975), pp. 126–137; and T. Stix, *Waves in Plasmas,* (American Institute of Physics, New York, 1992), pp. 74–78.

[21] See, for example, the last reference in Ref. 20, Chapter 10.

[22] H. Berk and D. L. Book, Phys. Fluids **12**, 649 (1969).